Dalton Transactions

Accepted Manuscript

ROYAL SOCIETY OF CHEMISTRY

www.rsc.org/dalton

Graphical Abstract

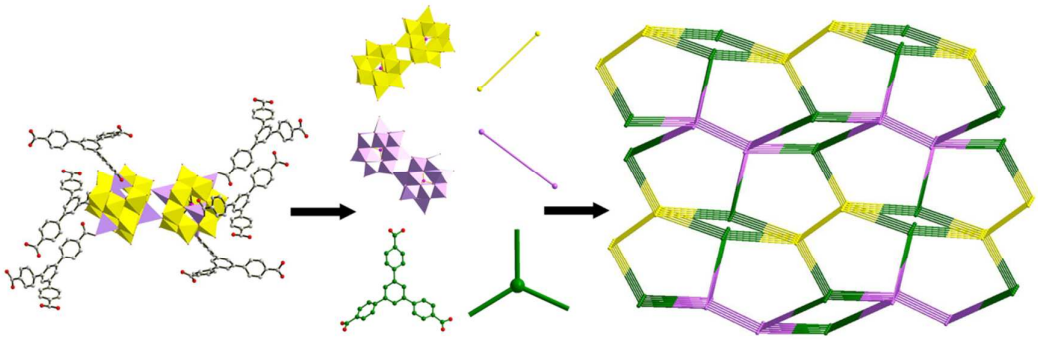

A 2-fold interpenetrated 3D porous POMOF with substantial catalytic activity towards bromate reduction was successfully isolated, which represents the first attempt to construct POMOF by using the methodology of extension the transition-metal-grafted ε-Keggin polyoxoanion with an expanded tripodal ligand H_3BTB.

Cite this: DOI: 10.1039/c0xx00000x

www.rsc.org/xxxxxx

ARTICLE TYPE

The First Tritopic Bridging Ligand 1,3,5-tris(4-carboxyphenyl)-benzene (H_3BTB) Functionalized Porous Polyoxometalate-Based Metal-Organic Framework (POMOF): From Design, Synthesis to Electrocatalytic Properties

Bao-xia Dong,*[a] Lu Chen,[a] Shi-yang Zhang,[a] Jun Ge,[a] Liang Song,[a] Hui Tian,[a] Yun-lei Teng*[a] and Wen-long Liu[a]

Received (in XXX, XXX) Xth XXXXXXXXX 20XX, Accepted Xth XXXXXXXXX 20XX
DOI: 10.1039/b000000x

Replacing the metal ions (or metal clusters) in the routine MOFs with size-matched polyoxoanions to construct POM-based MOF materials (POMOF) combining well-defined crystalline structures, high surface areas, regular and tunable cavities is the great challenge in current POM chemistry area. In this work, we report a 2-fold interpenetrated porous POMOF, $[TBA]_6[H_3PMo_{12}O_{40}]_2[Zn_8(BTB)_2]\cdot(\sim 35H_2O)$, which exhibits effective catalytic activity towards bromate reduction, by using the methodology of extension the reduced transition-metal-grafted ε-Keggin polyoxoanions with an expanded tripodal bridging ligand of H_3BTB. The simultaneous TGA/DSC-MS technique was applied in this work to identify the evolved gases and was proved to be an effective method for analysising the decomposition process.

Introduction

Owing to their permanent porosity, high surface area, large pore volume, and adjustable pore size and shape, metal-organic frameworks (MOFs) have been extensively investigated in the past decades and have shown promising applications in gas storage, separation and heterogeneous catalysis.[1] Their potential commercial applications are usually limited by the weak thermal and chemical stabilities, which are the critical properties for commercial sorbents.[1a] For instance, MOFs have in rare instances displayed thermal stability up to 500 ºC.[2] Besides, most MOFs, in particular zinc-based MOFs, are moisture-sensitive because the relative weak metal-oxygen coordiantion allows for attack by water molecules, resulting in the phase transformation and decomposition of the framework.[3] As a result, much care must be taken (*e.g.* operation in glove box) to avoid the structural collapse of MOFs. It is clearly beneficial to discover new high-surface area MOFs that are stable toward diverse environments such as air, water, acidic and basic media, and even extreme temperatures and pressures.

Polyoxometalates (POMs), as an outstanding class of structure-tunable building blocks with unrivaled versatility,[4] could combine with various inorganic linkers or metal-organic bridges to form POM-upholding or POM-templated frameworks.[5] Typically, MOFs are built by the self-assembly of metal ions or polynuclear metal clusters and polytopic bridging ligands under solvothermal conditions. Replacing the metal ions (or metal clusters) in the routine MOFs with size-matched polyoxoanions to construct POM-based MOF materials (POMOF) combining well-defined crystalline structures, high surface areas, regular and tunable cavities is the great challenge in current POM chemistry area.[5a] Beside the structural versatility, POM materials are endowed with paticular multifunctionalities, for example, strong brønsted acidity, reversible redox properties, high stability and high catalytically active site density.[6] Blending of distinctively different components of MOFs and POMs, provide a new pathway for incorporating catalytically active sites in a chemical stable porous framework, which demonstrates great potential for applications in diverse fields such as selective adsorption, catalysis and electrocatalysis.[7]

Up to now, there are three prime approaches for constructing porous POMOFs: (a) preparation of POM-loaded MOF materials by immobilizing POM anions within nanocages of the MOFs framework, *i.e.* MIL-100 or MIL-101;[8] (b) preparation of POM-encapsulated MOF single-crystal materials by using the template role of POM anions,[5a-5e,9] for example, the non-coordinating guests of Keggin anions templated host matrix with cuboctahedral cages like HKUST-1;[9a-d] (c) preparation of POM-based MOF single-crystal materials by using the coordination ability of POM anions. In this case, several noteworthy studies based on M-ε-Keggin ($M=Zn^{II}$, Ni^{II}, La^{III}) by Dolbecq *et al,*[10] and $Ni_6(\mu_3\text{-}OH)_3\text{-}XW_9O_{34}$ by Yang *et al*,[11] are published. A preliminary effective way for designing new POM-based MOF materials has been established through the extension of the transition-metal-grafted or transition-metal-substituted POM anion by bridging organic linkers such as 1,3-benzenedicarboxylate,[10e] 1,4-benzenedicarboxylate,[10b] 1,3,5-benzenetricarboxylate,[10d-e] 1,2,4-benzenetricarboxylate[11a] and 1,2,4,5-benzenetetracarboxylic acid,[10a] etc.

With the introducing of tritopic 1,3,5-benzenetricarboxylate ligand into the tetrahedral Zn_4-ε-Keggin system, a porous (3,4)-connected network of **ofp**-like POMOF with 72% solvent-accessible voids, $\varepsilon(trim)_{4/3}$ was isolated.[10d] In comparison with that of the preferred nets **ctn** and **bor**, which are generated by the combination of triangles and tetrahedra with a strict alternation, **ofp** topology shows higher density as a result of a higher stability. Yaghi *et al* proposed that frameworks with large pores can be realized if vertexes in a network are spaced apart by longer links to give expanded structures without changing the topology.[12] As inspired by their pioneering work of reticular chemistry in MOFs, we thus envision that it would be possible to construct microporous POM-upholding metal-organic frameworks by rational selecting the expanded polytopic carboxylate to react with the M-ε-Keggin moiety. We present herein the extension of the transition-metal-grafted ε-Keggin polyoxoanion by using an expanded tripodal bridging ligand of H_3BTB (1,3,5-tris(4-carboxyphenyl)-benzene). From this reaction system, we obtained an unexpected 2-fold interpenetrated 3D network based on a reduced $\{\varepsilon\text{-}H_3PMo^{V}_{8}Mo^{VI}_{4}O_{40}Zn_4\}_2$ dimer, $[TBA]_6[H_3PMo^{V}_{8}Mo^{VI}_{4}O_{40}]_2[Zn_8(BTB)_2]\cdot(\sim 35H_2O)$ (**1**), which exhibits effective catalytic activity towards bromate reduction. To our knowledge, no reliable design of POM-based porous materials from this approach has yet been reported to date.

Experimental

Materials and General Methods.

All chemicals purchased were of reagent grade and were used as received. H_3BTB was synthesized according to a documented procedure by 1,3,5-tri(4-methylphenyl)benzene.[13] FTIR spectrum (KBr pellets) was recorded in range of 4000−400 cm^{-1} on a BRUKER TENSOR 27 Fourier-transform infrared spectrometer. TGA/DSC-MS measurement (TGA, Thermal gravimetric analyses; DSC, Differential Scanning Calorimetry; MS, Mass Spectrometry) were performed on a TG/DSC Model STA 449 F3 Netzsch instrument at a ramp rate of 5 ºC min^{-1} and a Aelos Model QMS 300 MS apparatus was used to identify the evolved gases, by heating the sample under argon. The UV absorption characteristics were measured on a Shimadzu UV-2550 UV-Vis spectrophotometer. Luminescence spectra of crystalline samples were measured on a Hitachi F-4500 spectrophotometer. Powder XRD data were collected with CuKα (λ=1.5406 Å) radiation on a Bruker-AXS D8 Advance X-ray diffractometer in the angular range 2θ =5°−50° at 298 K. Each pattern is recorded with a 2 s per step scan.

Synthesis of $[TBA]_6[H_3PMo_{12}O_{40}]_2[Zn_8(BTB)_2]\cdot(\sim 35H_2O)$ (1).

10.0 mL of distilled water was added to a beaker, which contains $Na_2MoO_4\cdot 2H_2O$ (1.26 g, 5.2 mmol), Mo powder (0.10 g, 1.04 mmol), $ZnCl_2$ (0.28 g, 2.0 mmol), H_3PO_3 (0.05g, 0.61 mmol), and Tetrabutylammonium hydroxide (TBAOH, 0.25 g, 0.90 mmol) with stirring for 20 min. Next, the pH value of the mixture was adjusted to 4.9 with 2 mol L^{-1} HCl and then the mixture was stirred for another 30 min followed by the addition of H_3BTB (0.13 g, 0.3 mmol). Then the mixture was transferred and sealed in a 23 mL Teflonlined stainless steel container, and heated at 180 °C for 3 days. After slow cooling to room temperature with the rate of 10 °C/h, dark red crystals **1** were collected and washed with deionized water, then dried in air. After sieving by a standard sieve of 250, crystals of **1** with size greater than 0.06 mm were collected with high purity (yield: ca.0.7 g, 50% based on Mo). Prominent FT-IR peaks for **1** (KBr Pellet, cm^{-1}): 3466m, 2956(m), 2868(m), 2399(w), 2302(w), 1603(m), 1471(m), 1372(m), 934(s), 817(s), 779(s), 708(m).

X-ray Crystallographic Study.

Single-crystal X-ray diffraction analysis data was collected on a Bruker Smart Apex CCD diffractometer with Mo Kα monochromated radiation (λ=0.71073 Å) at room temperature. The structure was solved by direct methods and refined on F^2 by full-matrix least-squares methods using the SHELXTL package. Anisotropic thermal parameters were used to refine all Mo, Zn, P, O (except disordered O22 and O90) atoms. All the C atoms in the BTB^{3-} ligand were anisotropically refined. Part of C and N atoms were isotropically refined to avoid resulting in the "non positive defines". Therefore, isotropic non-H atoms in main residue were reported with 29 in checkcif. After locating and refining the hybrid POM and TBA, the difference Fourier map showed many peaks of very low electronic density, suggesting an extensive disordered of the water solvent molecules. Thus, the solvent molecules reside in those regions of diffuse electron density were treated by the PLATON/SQUEEZE procedure,[14] which suggested a unit cell accessible volume of 1407.3 $Å^3$ (about 12.2%), which could accommodate about 35 water molecules per formula unit. The structure was then refined again using the generated solvent-free diffraction data. Sensible restraints (including DFIX, ISOR, SIMU, DELU) were used confine the C–N and C–C bond with similar lengths, and to confine the temperature factors as well as Hirshfeld differences. The hydrogen atoms attached to carbon positions were placed in geometrically calculated positions. Hydrogen atoms attached to the disordered C atoms and the bridging oxygen atoms (O19, O21, O24, O62, O66 and O86) were not located but included in the structural formula because of the charge balance requirements. The crystal data and structure refinement results of squeezed compound **1** are summarized in Table S1. Selected bond lengths and angles are listed in Tables S2 and S3, respectively. Crystallographic data for the structure reported in this paper has been deposited in the Cambridge Crystallographic Data Center with CCDC number 1011903 for **1**.

Electrochemical Studies.

A CHI 600a Electrochemical Workstation connected to a computer was used for control of the electrochemical measurements and for data collection. A conventional three-electrode system was used. The working electrode was a modified CPE. An Ag/AgCl (saturated KCl) electrode was used as a reference electrode and Pt gauze as a counter electrode. All potentials were measured and reported versus the Ag/AgCl electrode. All experiments were performed at room temperature.

Electrode Preparation.

POMOF-CPE (POMOF carbon paste electrode) was used to assess the solid-state electrochemical behavior of the POMOF. It was prepared as follows: 200 mg graphite powder and 30 mg compound **1** were mixed and ground together by agate mortar to achieve a uniform and dry mixture; to the mixture 0.1 mL mineral oil was added and stirred with a glass rod; then the homogenized

mixture was used to pack 3 mm inner diameter glass tube and pressed tightly with a copper rod through the back of the electrode. The electrode surface was smoothed in the bottom of agate mortar.

Results and Discussion

Description of the Crystal Structures.

Single-crystal X-ray diffraction analysis revealed that compound **1** crystallizes in the triclinic *P-1* space group and is based on a reduced ε-Keggin core (Figure S1), that is, {ε-$H_3PMo^{V}_8Mo^{VI}_4O_{40}$}. The asymmetric unit contains two different ε-Keggin anions (ε-Keggin 1 and ε-Keggin 2), eight crystallographically independent Zn^{II} centers, two BTB^{3-} ligands, six TBA^+ counter cations (Figure S2). It is noted that the POM building unit of compound **1** is not the expected four-capped Zn_4-ε-Keggin POM, but a dimerized form of this POM, as shown in Figure S1. In such dimer, two Zn_4-ε-Keggin units are linked via two Zn–O bonds (Zn4–O16, 1.943 (7) Å in ε-Keggin 1 and Zn5–O54, 1.932(7) Å in ε-Keggin 2) between one capping Zn ion on a POM and a bridging oxygen atom of a neighboring POM. Such dimerization leaves six anchoring points for each dimer. Each anchoring point is further linked by one BTB ligand using one carboxylate group in it in a monodentate coordination mode (Figure 1a). Such structure of the dimeric unit evokes the staggered conformation of ethane, as observed in the structure of imidazole and benzenetricarboxylate derivatives reported by Dolbecq *et al.*[10c-d]

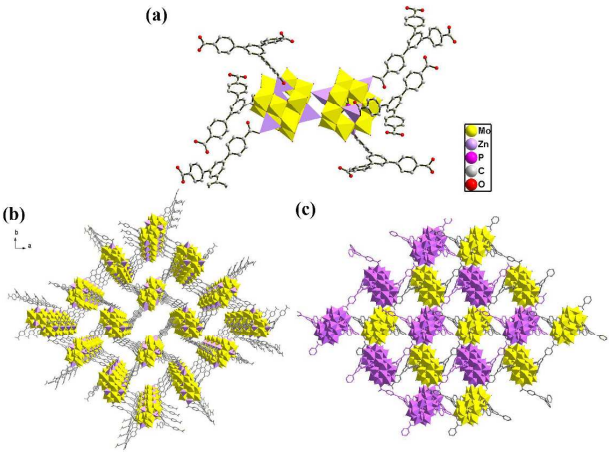

Figure 1. Polyhedral representations of (a) the six-coordinated POM dimer (referred to the ε-Keggin 1) and (b) the single 3D framework as well as (c) the two-fold interpenetrated framework of **1** along c axis.

The connection of the dimeric POMs via the BTB linkers generates a 3D framework with ~22 Å × 10 Å, ~15 Å × 8 Å and ~ 11 Å × 10 Å channels in the *ab*, *bc* and *ac* planes, respectively (Figure 1b and Figure S3), in which each carboxylate group of the BTB adopts a monodentate coordination mode. A single 3D network incorporates with one other identical network giving rise to a 2-fold interpenetrating network (Figure 1c). Such interpenetrated framework maintains microporous properties in the *ab* plane and *bc* plane with the channel dimensions of ~8 Å × 8 Å and ~15 Å × 8 Å, respectively (Figure S4) if omitting the TBA^+ and water molecules inside the channels. As thus 59.7% of the total solvent-accessible volume of **1** is gotten as estimated by PLATON calculation.

It should be noted that there are two crystallographically independent ε-Keggin anions and two types of BTB^{3-} ligands in the asymmetric unit. Both of the two types of ε-Keggin form the dimer of Zn_8-ε-$(H_3PMo_{12}O_{40})_2$ which are labelled as Dimer-1 and Dimer-2. Both of the BTB ligands (BTB-1 and BTB-2) adopt the tri-monodentate coordination mode linking with three Zn^{II} centers (Zn1, Zn5 and Zn6 for BTB-1, Zn2, Zn3 and Zn7 for BTB-2). After careful examination of the structures we found that three apical benzene rings and the central benzene ring are not coplanar in both BTB ligands, which show *ca.* 42.2, 30.6, 27.1º (in BTB-1) and *ca.* 47.7, 45.0, 35.0º (in BTB-2) for the angles between planes (Figure S5). Concerning to the linking of POM-Metal-Ligand, each Dimer-1 is coordinated by two BTB-1 and four BTB-2 molecules, while each Dimer-2 is coordinated by four BTB-1 and two BTB-2 molecules (Figure S6). As shown from Figure 2a, BTB-2 molecules exert the bridging role extending the linkage to form a plane while BTB-1 molecules extending the linkage in the vertical direction of the plane (Figure S7). Different dimers in the plane are distributed alternately. Through such connection, a single (3,4-connected) 3D framework is generated (Figure 2b).

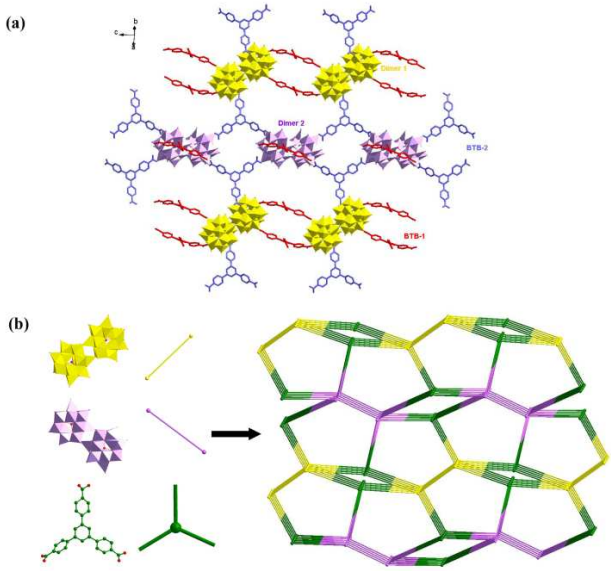

Figure 2. (a) Representation of the connections between different BTB molecules and dimers in a plane; (b) Schematic view of the 3D topology of **1**.

PXRD, BET and TGA/DSC-MS.

The chemical resistance of compound **1** was examined by suspending samples in aqueous HCl or NaOH solutions at pH from 1 to 11. Remarkably, compound **1** is stable up to pH 10 and maintains its crystallinity after 4 hours immersion, which is confirmed by PXRD data collected before and after each test (Figure S8). For the peaks of *2θ* from 5 to 10 with stronger intensity, no major change but only the change of intensities was observed, which is reasonably due to the difference in solvent contents. Besides, for the samples which have been immersed in pH=1, 4 and 10 solutions for 4 hours, the relative intensity of the

stronger diffraction peaks at 2θ = 5.56, 6.61 and 7.53 recovered once they were suffered further immersion in deionized water for another 4 hours.

Compound **1** was desolvated by heating at 250 °C overnight under high vacuum and N_2 adsorption isotherm was collected at 77 K with a Brunauer–Emmett–Teller (BET) surface area of 47.5 $m^2\ g^{-1}$ (Langmuir surface area of 133.2 $m^2\ g^{-1}$, Figure S9). The bulk-phase purity and its structural chemical integrity at 250 °C were confirmed by PXRD (Figure S10).

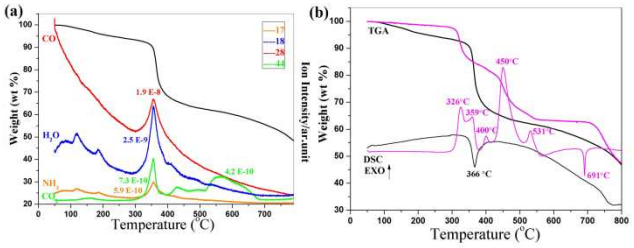

Figure 3. (a) TGA/MS data recorded in argon for compound **1**; (b) The TGA/DSC curves for compound **1** in Air (pink) and Argon (black) atmospheres, respectively.

Thermogravimetric analysis of compound **1** was carried out in argon atmosphere with a heating rate of 5 °C min^{-1} in the temperature range from 50 to 800 °C. It shows consecutive weight loss stages in the whole temperature range. The simultaneous TGA/DSC-MS data (Figue 3a) for the volatiles evolved from **1** indicates that, in the range of 50–300 °C, masses 17 (NH_3), 18 (H_2O) and 44 (CO_2) were desorbed from the sample, which corresponding to the release of the lattice water and the complete combustion of two TBA^+ to generate NH_3, CO_2 and H_2O. When temperature above 300 °C, most of these volatiles were desorbed, which include the complete combustion products of NH_3, H_2O, CO_2 (combustion of TBA^+ and BTB^{3-}) and the incomplete combustion products of CO (28). The release of a great quantity of reductive gases of CO helps us to draw a conclusion that reduction reaction was happened during the decomposition of the sample. Assuming the residue corresponds to reductive products of Zn and Mo, the calculated reside should be 43.31%. Since no plateau was observed in the TGA curve in argon atmosphere, a repeated analysis in air atmosphere with same heating rate was carried out, as shown from Figure 3b. It shows five distinct weight losses in the range of 50–600 °C. Assuming the residue corresponds to the oxidized products of ZnO and MoO_3, the observed reside 63.21% is in good agreement with the calculated value of 62.94%. Therefore, the TGA results indicate only two water molecule was lost in the range of 50–250 °C (0.5%), which is much less than the PLATON/SQUEEZE calculated one of 35. In comparison of the DSC curves in different atmospheres, the solely endothermic peak at 366 °C in agron indicates a decomposition and gasification process, while three moderate exothermic peaks at 326, 359, 400 °C indicate the oxidation processes for the TBA. A sharp exothermic peak at 450 °C indicates the oxidation process for the remaining TBA^+ and BTB^{3-} molecules. A further exothermic peak at 531 °C could be attributed to the collapse of the POM and the last endothermic peak at 691 °C is attributed to the melting point peak of MoO_3.

Electrochemical and Electrocatalysis.

The Keggin-type POMs are known to exhibit well defined redox waves and are usually considered to be electron reservoirs.[15] One of their domains of application thus concerns electrocatalysis.[16] Bromate, a disinfection by-product, is formed when ozone (used to disinfect drinking-water) reacts with naturally occurring bromide in drinking water.[17] BrO_3^- ions are suspected to act as carcinogens that may cause a range of cancers.[18] Electrochemical reduction of bromate provides a suitable method for its determination and removal from aqueous media since it is relatively clean, environment-friendly and cost efficient.[19] The solid-state electrochemistry was carried out by entrapping the POMOF in a CPE. Cyclic voltammograms (CVs) of **1**-CPE in the potential region of −150 to +600 mV at different scan rates are presented in Figure 4a which exhibit three pairs of redox peaks, I–I′, II–II′ and III–III′, featuring three consecutive bielectronic processes as described by Eq. (1)–(3).[10e] The half-wave potentials $E_{1/2}$ are 353, 229 and 45 mV, respectively ($E_{1/2} = (E_{pa} + E_{pc}) / 2$; E_{pa} and E_{pc} are the anodic and cathodic peak potentials, scan rate: 50 mV/s). The peak currents are proportional to the scan rates up to 200 mV/s, which indicates that the redox process of **1**-CPE is surface-controlled (Figure S11). Furthermore, with increasing pH, the redox potentials all gradually shift to negative direction and the peak currents decrease (Figure S12). This phenomenon is consistent with the fact that the reduction of **1**-CPE is accompanied by the evolution of protons from solution to the electrode surface to maintain charge neutrality.[20] Along with increasing pH, slower penetration of protons to the ε-Keggin cluster anion should be the reason for the current decrease, the more negative reduction potentials can be explained by *Nernst* equation.[21]

$$[H_3PMo_{12}O_{40}]^{8-}(surf) + 2\ H^+ + 2e^- \rightleftharpoons [H_5PMo_{12}O_{40}]^{8-}(surf) \quad (1)$$

$$[H_5PMo_{12}O_{40}]^{8-}(surf) + 2\ H^+ + 2e^- \rightleftharpoons [H_7PMo_{12}O_{40}]^{8-}(surf) \quad (2)$$

$$[H_7PMo_{12}O_{40}]^{8-}(surf) + 2\ H^+ + 2e^- \rightleftharpoons [H_9PMo_{12}O_{40}]^{8-}(surf) \quad (3)$$

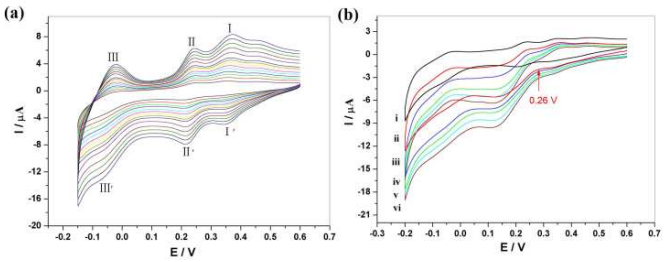

Figure 4. (a) Cyclic voltammograms and peak current intensity variations for **1**-CPE in a 1 M H_2SO_4 medium. Scan rates from inner to outer curve: 20, 30, 40, 50, 60, 70, 80, 90, 100, 120, 140, 160, 180 and 200 mV s^{-1}, respectively. (b) Cyclic voltammograms in a 1 M H_2SO_4 solution in the absence (i) and presence of (ii) 1.0 mM, (iii) 2.0 mM, (iv) 3.0 mM, (v) 4.0 mM and (vi) 5.0 mM of BrO_3^-. Scan rate= 80 mV s^{-1}. The reference electrode was an Ag/AgCl electrode.

The catalytic activity of **1**-CPE towards BrO_3^- reduction was examined, as shown in Figure 4b. In aqueous 1.0 M H_2SO_4 media, upon addition of 1.0 mM of BrO_3^-, a dramatic change in the shape of the voltammograms accompanies the electrocatalytic reduction. CVs data indicate that the initially reduced form, $[H_5PMo_{12}O_{40}]^{8-}$ (surf), exhibits minimal catalytic activity. In contrast, the second reduced form, $[H_7PMo_{12}O_{40}]^{8-}$ (surf), which

commences at around 0.26 V, induces considerable catalytic activity. An increase in current also was detected at potentials relevant to the third reduction process (III′). The current plateaus observed in the potential regions corresponding to the second and third reduction processes, suggest that the reduced forms of ε-Keggin formed in these reactions both exhibit effective catalytic activity towards bromate reduction. The catalytic reduction current increases when the concentration of BrO_3^- increases from 1.0 to 5.0 mM. The reaction mechanism of reduction of BrO_3^- involving a six-electron process, yielding bromide (Br^-) as a final product, as proposed with other POMs in the literature.[22] The effect of pH on the electrocatalytic reduction of bromate on **1**-CPE was studied in H_2SO_4 media at pH values over the range of 1 to 5. As shown in Figure S13, peak shaped voltammograms were almost retained. With the peak potentials for bromate reduction shifting to more negative values with increasing pH, the peak current magnitude decreases, which indicates that the bromate reduction strongly depends on the acidity.[23]

Conclusions

In summary, compound **1** represents the first example of expanded tripodal bridging ligand H_3BTB functionalized porous POMOF. The building block is composed of a dimerized form of transition metal grafted Zn_4-ε-Keggin polyoxanion, which is further linked by tritopic H_3BTB ligand in a staggered ethane style to form a 3D topology. The successful isolation of **1** confirms the feasibility of the methodology that extension transition-metal-grafted Keggin by rational selecting of tripodal bridging carboxylate ligand to construct new porous POMOFs. Replacing the Zn_4-ε-Keggin building block with other size-matched and catalytically active polyoxoanions or choosing suitable tripodal bridging carboxylate ligands provide a promising pathway for constructing POMOFs with great potential for applications in selective adsorption, catalysis and electrocatalysis. Such work is undergoing in our group.

Acknowledgements

This work is financially supported by the NNSF of China (No. 21301152, 21371150).

Notes and references

[a] *College of Chemistry and Chemical Engineering, Yangzhou University, Yangzhou, Jiangsu 225002, P. R. China. Fax: +86 51487975590-9201; Tel: +86 51487975590-9201; E-mail: bxdong@yzu.edu.cn (B-X. Dong); ylteng@yzu.edu.cn (Y-L. Teng).*

† Electronic Supplementary Information (ESI) available: [Crystal data for 1 (CIF); details of characterization (PXRD, IR, UV, FL, CV and views of the structures).].See DOI: 10.1039/b000000x/

1 (*a*) H. Furukawa, K. E. Cordova, M. O'Keeffe and O. M. Yaghi, *Science*, 2013, **341**, 1230444–1; (*b*) 2012 metal-organic frameworks issue. *Chem. Rev.*, 2012, **112**, 673–1268; (*c*) S. Hasegawa, S. Horike, R. Matsuda, S. Furukawa, K. Mochizuki, Y. Kinoshita and S. Kitagawa, *J. Am. Chem. Soc.*, 2007, **129**, 260; (*d*) R.-Q. Zou, H. Sakurai, S. Han, R.-Q. Zhong and Q. Xu, *J. Am. Chem. Soc.*, 2007, **129**, 8402.

2 (*a*) K. S. Park, Z. Ni, A. P. Côté, J. Y. Choi, R. Huang, F. J. UribeRomo, H. K. Chae, M. O'Keeffe and O. M. Yaghi, *Proc. Natl. Acad. Sci. U. S. A.*, 2006, **103**, 10186; (*b*) T. Loiseau, C. Huguenard, G. Fink, F. Taulelle, M. Henry, T. Bataille and G. Férey, *Chem. Eur. –J.*, 2004, **10**, 1373; (*c*) V. Colombo, S. Galli, H. J. Choi, G. D. Han, A. Maspero, G. Palmisano, N. Masciocchi and J. R. Long, *Chem. Sci.*, 2011, **2**, 1311.

3 (*a*) S. S. Kaye, A. Dailly, O. M. Yaghi and J. R. Long, *J. Am. Chem. Soc.*, 2007, **129**, 14176; (*b*) J. A. Greathouse and M. D. Allendorf, *J. Am. Chem. Soc.*, 2006, **128**, 10678; (*c*) J. J. Low, A. I. Benin, P. Jakubczak, J. F. Abrahamian, S. A. Faheem and R. R. Willis, *J. Am. Chem. Soc.*, 2009, **131**, 15834.

4 (*a*) C. L. Hill, *Chem. Rev.*, 1998, **98**, 1–2; (*b*) L. Cronin and A. Müller, *Chem. Soc. Rev.*, 2012, **41**, 7333–7334.

5 (*a*) D.-Y. Du, J.-S. Qin, S.-L. Li, Z.-M. Su and Y.-Q. Lan, *Chem. Soc. Rev.*, 2014, **43**, 4615; (*b*) M. Wei, C. He, W. Hua, C. Duan, S. Li and Q. Meng, *J. Am. Chem. Soc.*, 2006, **128**, 13318; (*c*) Z.-Y. Fu, Y. Zeng, X.-L. Liu, D.-S. Song, S.-J. Liao and J.-C. Dai, *Chem. Commun.*, 2012, **48**, 6154; (*d*) C. Zou, Z. Zhang, X. Xu, Q. Gong, J. Li and C.-D. Wu, *J. Am. Chem. Soc.*, 2012, **134**, 87; (*e*) Y. Ishii, Y. Takenaka and K. Konishi, *Angew. Chem. Int. Ed.*, 2004, **43**, 2702; (*f*) H. N. Miras, L. Vilà-Nadal and L. Cronin, *Chem. Soc. Rev.*, 2014, **43**, 5679; (*g*) Z.-X. Zhang, M. Sadakane, T. Murayama and W. Ueda, *Dalton Trans.*, 2014, **43**, 13584; (*h*) Z.-X. Zhang, M. Sadakane, T. Murayama, N. Sakaguchi and W. Ueda, *Inorg. Chem.*, 2014, **53**, 7309; (*i*) Z.-X. Zhang, M. Sadakane, T. Murayama, S. Izumi, N. Yasuda, N. Sakaguchi and W. Ueda, *Inorg. Chem.*, 2014, **53**, 903.

6 (*a*) A. Müller, M. T. Pope, F. Peters and D. Gatteschi, *Chem. Rev.*, 1998, **98**, 239; (*b*) E. Coronado, J. R. Galán-Mascarós, C. Giménez-Saiz, C. J. Gómez-García, E. Martínez-Ferrero, M. Almeida and E. B. Lopes, *Adv. Mater.*, 2004, **16**, 324.

7 (*a*) S. Uchida, R. Eguchi, S. Nakamura, Y. Ogasawara, N. Kurosawa and N. Mizuno, *Chem. Mater.*, 2012, **24**, 325; (*b*) E. V. Ramos-Fernandez, C. Pieters, B. van der Linden, J. Juan-Alcañiz, P. Serra-Crespo, M. W. G. M. Verhoeven, H. Niemantsverdriet, J. Gascon and F. Kapteijn, *J. Catal.*, 2012, **289**, 42.

8 (*a*) R. Canioni, C. Roch-Marchal, F. Sécheresse, P. Horcajada, C. Serre, M. Hardi-Dan, G. Férey, J. M. Grenèche, F. Lefebvre, J. S. Chang, Y. K. Hwang, O. Lebedev, S. Turnerf and G. V. Tendeloo, *J. Mater. Chem.*, 2011, **21**, 1226; (*b*) O. A. Kholdeeva, N. V. Maksimchuk and G. M. Maksimov, *Catal. Today*, 2010, **157**, 107.

9 (*a*) C.-Y. Sun, S.-X. Liu, D.-D. Liang, K.-Z. Shao, Y.-H. Ren and Z.-M. Su, *J. Am. Chem. Soc.*, 2009, **131**, 1883; (*b*) F. Ma, S. Liu, D. Liang, G. Ren, C. Zhang, F. Wei and Z. Su, *Eur. J. Inorg. Chem.*, 2010, 3756; (*c*) F.-J. Ma, S.-X. Liu, C.-Y. Sun, D.-D. Liang, G.-J. Ren, F. Wei, Y.-G. Chen and Z.-M. Su, *J. Am. Chem. Soc.*, 2011, **133**, 4178; (*d*) J. Song, Z. Luo, D. K. Britt, H. Furukawa, O. M. Yaghi, K. I. Hardcastle and C. L. Hill, *J. Am. Chem. Soc.*, 2011, **133**, 16839; (*e*) S. Uchida, N. Mizuno, *Coord. Chem. Rev.*, 2007, **251**, 2537–2546; (*f*) C.-J. Jiang, A. Lesbani, R. Kawamoto, S. Uchida and N. Mizuno, *J. Am. Chem. Soc.*, 2006, **128**, 14240; (*g*) S. Uchida, M. Hashimoto and N. Mizuno, *Angew. Chem. Int. Ed.*, 2002, **41**, 2814.

10 (*a*) A. Dolbecq, C. Mellot-Draznieks, P. Mialane, J. Marrot, G. Férey and F. Sécheresse, *Eur. J. Inorg. Chem.*, 2005, 3009; (*b*) L. M. Rodriguez-Albelo, A. R. Ruiz-Salvador, A. Sampieri, D. W. Lewis, A. Gómez, B. Nohra, P. Mialane, J. Marrot, F. Sécheresse, C. Mellot-Draznieks, R. N. Biboum, B. Keita, L. Nadjo and A. Dolbecq, *J. Am. Chem. Soc.*, 2009, **131**, 16078; (*c*) L. M. Rodriguez-Albelo, A. R. Ruiz-Salvador, D. W. Lewis, A. Gómez, P. Mialane, J. Marrot, A. Dolbecq, A. Sampieri and C. Mellot-Draznieks, *Phys. Chem. Chem. Phys.*, 2010, **12**, 8632; (*d*) B. Nohra, H. E. Moll, L. M. R. Albelo, P. Mialane, J. Marrot,C. Mellot-Draznieks, M. O'Keeffe, R. N. Biboum, J. Lemaire, B. Keita, L. Nadjo and A. Dolbecq, *J. Am. Chem. Soc.*, 2011, **133**, 13363; (*e*) L. M. Rodriguez-Albelo, G. Rousseau, P. Mialane, J. Marrot, C. Mellot-Draznieks, A. R. Ruiz-Salvador, S. Li, R. Liu, G. Zhang, B. Keita and A. Dolbecq, *Dalton Trans.*, 2012, **41**, 9989.

11 (*a*) S.-T. Zheng, J. Zhang, G.-Y. Yang, *Angew. Chem., Int. Ed.*, 2008, **47**, 3909; (*b*) S.-T. Zheng, J. Zhang, X.-X. Li, W.-H. Fang and G.-Y. Yang, *J. Am. Chem. Soc.*, 2010, **132**, 15102.

12 (*a*) O. M. Yaghi and Q.-W. Li, *MRS Bull.*, 2009, **34**, 682; (*b*) M. Eddaoudi, J. Kim, N. Rosi, D. Vodak, J. Wachter, M. O'Keeffe, O. M. Yaghi, *Science*, 2002, **295**, 469.

13 J. Kim, B. Chen, T. M. Reineke, H. Li, M. Eddaoudi, D. B. Moler, M. O'Keeffe and O. M. Yaghi, *J. Am. Chem. Soc.*, 2001, **123**, 8239.
14 A. L. Spek, *J. Appl. Crystallogr.*, 2003, **36**, 7.
15 M. Sadakane and E. Steckhan, *Chem. Rev.*, 1998, **28**, 219.
16 B. Keita and L. Nadjo, *J. Mol. Catal. A*, 2007, **262**, 190.
17 K. M. Crofton, *Toxicology*, 2006, **221**, 212.
18 T. Umemura and Y. Kurokawa, *Toxicology*, 2006, **22**, 154.
19 L. Ding, Q. Li, D.-D. Zhou, H. Cui, H. An and J.-P. Zhai, *J Electroanal Chem*, 2012, **668**, 44.
20 C. M. A. Brett and A. M. O. Brett, *Electrochemistry Principles, Methods, and Applications*, Oxford University, 1993.
21 J. Wang, *Analytical Electrochemistry*, VCH, New York , 1994.
22 (*a*) S. S. Hassan, Y.-P. Liu, Sirajuddin, A. R. Solangi, A. M. Bond and J. Zhang, *Anal. Chim. Acta*, 2013, **803**, 41; (*b*) L. Ding, Y.-P. Liu, S.-X. Guo, J.-P. Zhai, A. M. Bond and J. Zhang, *J Electroanal Chem*, 2014, **727**, 69.
23 X.-D. Xi and S.-J. Dong, *Electrochim Acta*, 1995, **40**, 2785.